N63-22945

NASA TECHNICAL NOTE

NASA TN D-2026

NASA TN D-2026

STATIC LONGITUDINAL AERODYNAMIC CHARACTERISTICS AND SURFACE PRESSURE DISTRIBUTIONS FOR A 1/15-SCALE MODEL OF A MODIFIED FOUR-STAGE SCOUT VEHICLE

by Thomas C. Kelly
Langley Research Center
Langley Station, Hampton, Va.

NATIONAL AERONAUTICS AND SPACE ADMINISTRATION • WASHINGTON, D. C. • OCTOBER 1963

TECHNICAL NOTE D-2026

STATIC LONGITUDINAL AERODYNAMIC CHARACTERISTICS AND SURFACE PRESSURE DISTRIBUTIONS FOR A 1/15-SCALE MODEL OF A MODIFIED FOUR-STAGE SCOUT VEHICLE

By Thomas C. Kelly

Langley Research Center
Langley Station, Hampton, Va.

NATIONAL AERONAUTICS AND SPACE ADMINISTRATION

NATIONAL AERONAUTICS AND SPACE ADMINISTRATION

TECHNICAL NOTE D-2026

STATIC LONGITUDINAL AERODYNAMIC CHARACTERISTICS AND SURFACE PRESSURE DISTRIBUTIONS FOR A 1/15-SCALE MODEL OF A MODIFIED FOUR-STAGE SCOUT VEHICLE

By Thomas C. Kelly

SUMMARY

Results have been obtained in the Langley 8-foot transonic pressure tunnel at Mach numbers from 0.60 to 1.20 for a 1/15-scale model of a modified four-stage launch vehicle. The investigation consisted of the determination of the static longitudinal characteristics for the complete vehicle and of the surface pressure distributions over the modified fourth-stage region at angles of attack from about -6° to 6°. The test Reynolds number per foot was approximately 3.7×10^{6}.

A comparison of results of the present investigation with those presented in NASA Technical Note D-794 for the original Scout vehicle indicates that enlargement of the fourth stage causes a slight general increase in the normal-force-curve slope, a more noticeable increase in the pitching-moment-curve slope, and a slight forward shift in the center-of-pressure location.

Measurements of the surface pressure distributions over the modified region indicate sizable variations of the negative pressure-coefficient peaks associated with the nose-cone—cylinder and cylinder—reverse-flare junctures with variations in Mach number or angle of attack. Examination of the results suggests the presence of increasingly negative section normal-force coefficients over the region of the reverse flare with increases in angle of attack.

INTRODUCTION

The Scout launch vehicle has been developed by the National Aeronautics and Space Administration for use in orbital missions, high-altitude probes, and reentry investigations. In support of the vehicle development program, a number of wind-tunnel investigations have been conducted to determine the aerodynamic force, moment, and loading characteristics for the Scout and for a number of related vehicles. Results of some of these investigations are available in references 1 to 7.

More recently, in order to permit the use of payloads of increased size, the fourth stage of the Scout was enlarged. This particular Scout vehicle is designated as the 34-inch-diameter heat-shield configuration. The present investigation was undertaken to determine the effects of this modification on the aerodynamic force and moment characteristics of the complete vehicle and on the aerodynamic loading characteristics of the enlarged fourth stage. The investigation was conducted in the Langley 8-foot transonic pressure tunnel at Mach numbers from 0.60 to 1.03 for the force-test results and from 0.60 to 1.20 for the pressure-distribution portion of the investigation. The angle-of-attack range extended from about -6° to 6°, and the average test Reynolds number per foot was approximately 3.7×10^{6}.

SYMBOLS

Aerodynamic force and moment data are referred to the body system of axes, with coefficients based on the maximum body cross-sectional area of 0.0388 square foot and the maximum body diameter of 2.668 inches. Moments are measured about a point located at 67.7 percent of the overall model length (measured from the theoretical nose-cone apex to the fin trailing edge).

C_A — axial-force coefficient, $\frac{\text{Axial force}}{qA}$

$C_{A,b}$ — base axial-force coefficient, $\frac{\text{Base axial force}}{qA}$

C_m — pitching-moment coefficient, $\frac{\text{Pitching moment}}{qAd}$

C_{m_α} — pitching-moment-curve slope, $\frac{\partial C_m}{\partial \alpha}$, per deg

C_N — normal-force coefficient, $\frac{\text{Normal force}}{qA}$

C_{N_α} — normal-force-curve slope, $\frac{\partial C_N}{\partial \alpha}$, per deg

C_p — pressure coefficient, $\frac{p_l - p}{q}$

A — maximum body cross-sectional area, 0.0388 sq ft

d — maximum body diameter, 2.668 in.

l — model overall length, measured from nose-cone apex to fin trailing edge, 60.15 in.

M — Mach number

p free-stream static pressure, lb/sq ft

p_l local static pressure, lb/sq ft

q free-stream dynamic pressure, lb/sq ft

R Reynolds number per foot

r radius of curvature, in.

x longitudinal distance, measured from theoretical nose-cone apex, in.

X_{cp} center-of-pressure location, measured in terms of maximum body diameters forward of model base

α angle of attack of body center line, deg

ϕ orifice row orientation angle, measured clockwise from vertical as viewed from front, deg

APPARATUS AND TESTS

Model

Details and design dimensions of the 1/15-scale modified Scout model are shown in figure 1(a). The cruciform fins, mounted with the trailing edge slightly

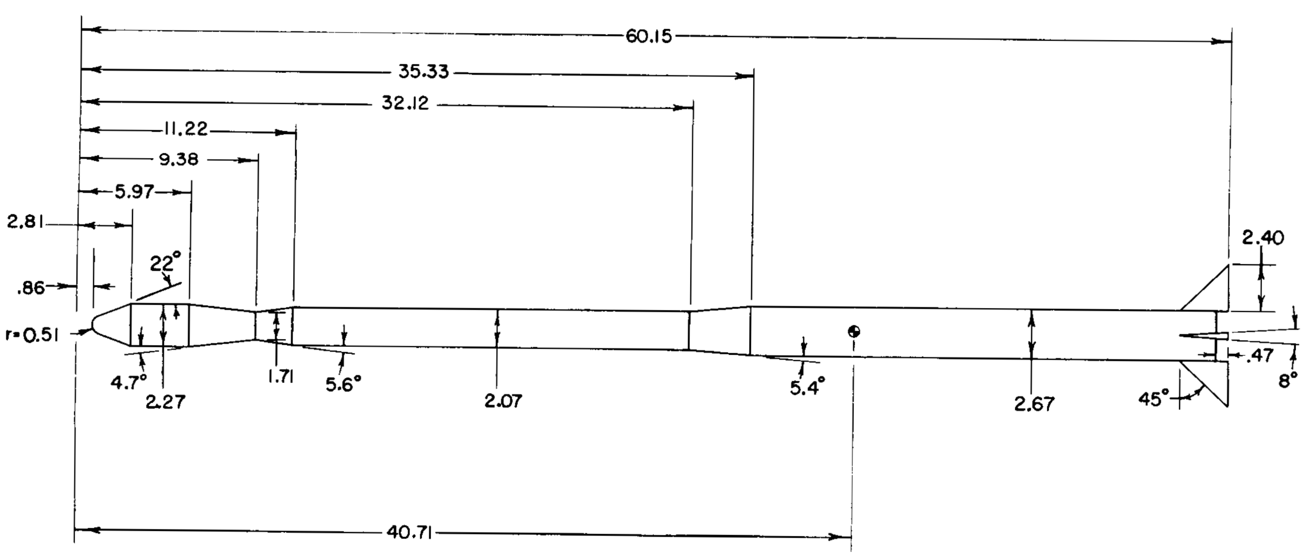

(a) Design dimensions, complete model.

Figure 1.- Model details. (All dimensions in inches.)

rearward of the first-stage base, have a leading-edge sweepback of 45° and employ single-wedge streamwise airfoil sections having an included angle of 8°. The fin leading edges were blunted, having a radius of curvature (measured normal to the leading edge) of 0.017 inch. As may be noted in figure 1, the model used for the present investigation was tested with the usual external protuberances (antennas, wiring conduits, and launch fittings) removed. (See ref. 4.)

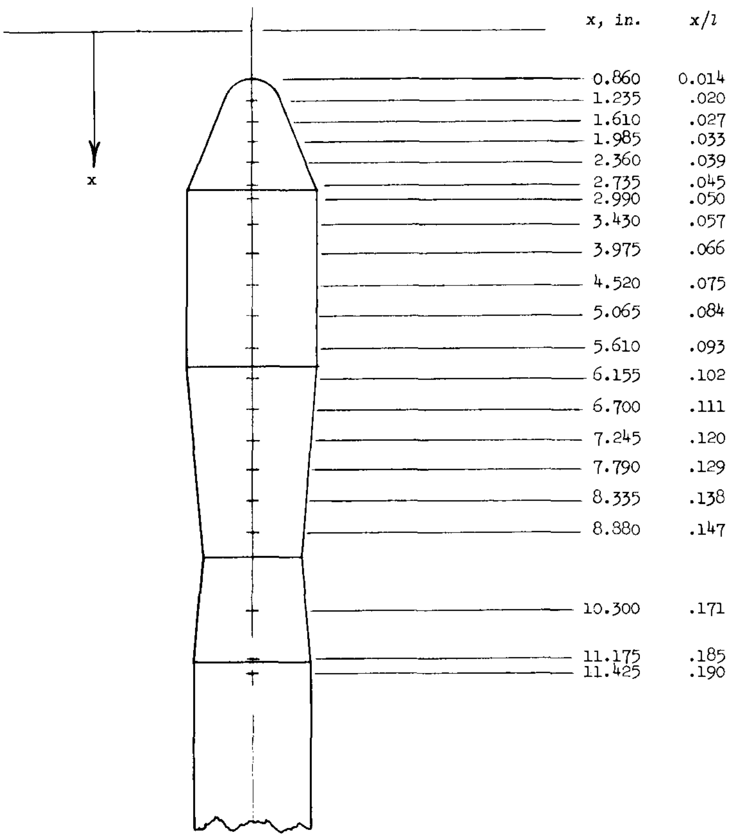

(b) Orifice locations, modified section.

Figure 1.- Concluded.

Pressure distributions were determined by using 21 orifices, which were installed in a single row extending from the nose rearward over the modified region. Orifice locations are given in figure 1(b), and model photographs are presented in figure 2.

A comparison of the model configuration of the present tests with the Scout model utilized for the investigation of reference 4 (configuration 215) indicates that the fourth-stage modification was accompanied by several incidental changes: The nose bluntness ratio, or the ratio of nose-cap radius to nose-cone base radius, was reduced from 0.60 to 0.45; the nose-cone half-angle was increased from 20° to 22°; and the overall length (model scale) was increased from 57.21 inches to 60.15 inches. For both the original and modified Scout models, the first stage, including the associated transition flare, and the location of the moment reference center relative to the model base were identical.

Tests and Procedure

As previously indicated, the investigation consisted essentially of two parts. During the first part, the longitudinal aerodynamic force and moment characteristics were determined for a 1/15-scale model of the complete vehicle through a Mach number range from 0.60 to 1.03. Effects of the first-stage fins were also determined during this part of the investigation. During the second part of the investigation, surface pressure distributions were measured over the modified region at Mach numbers from 0.60 to 1.20. In order to provide information necessary to determine section normal-force coefficients (not presented), the model was tested

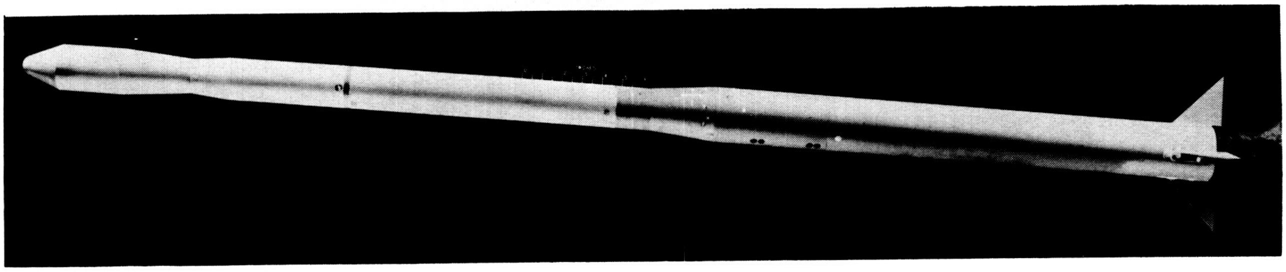

(a) Complete configuration. L-63-3832

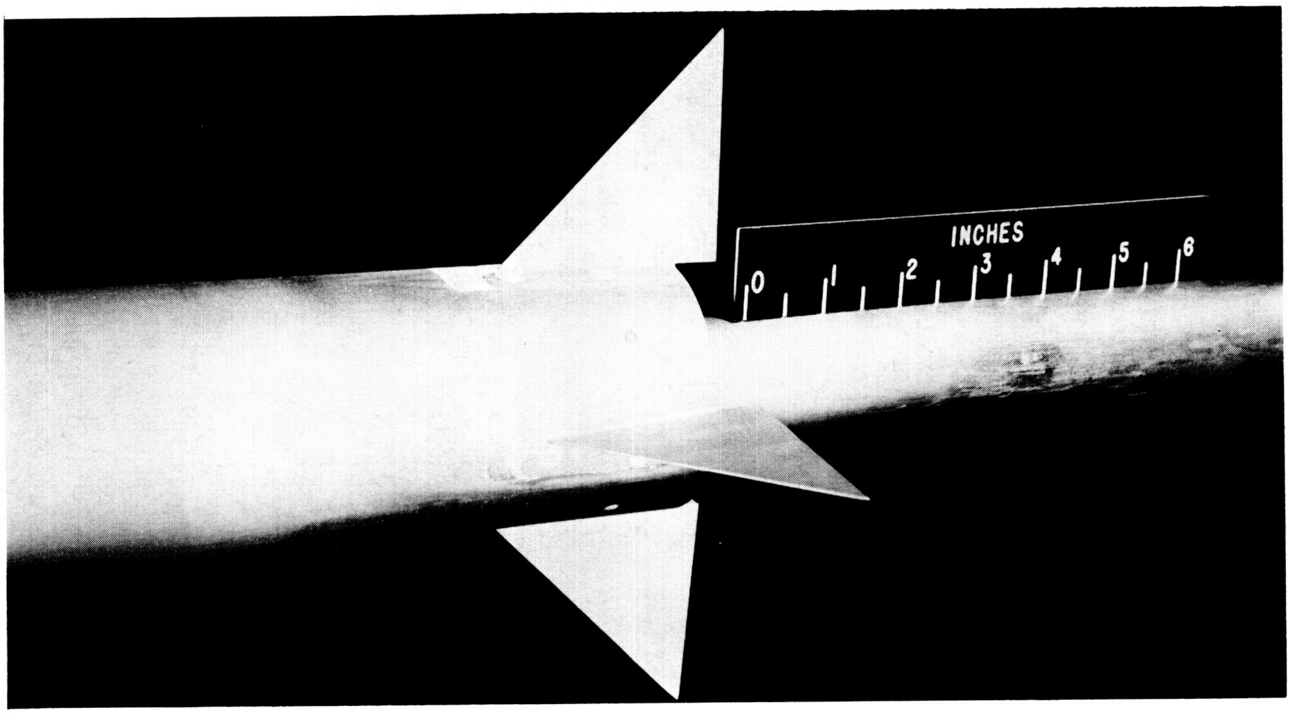

(b) Base fin details. L-63-3831

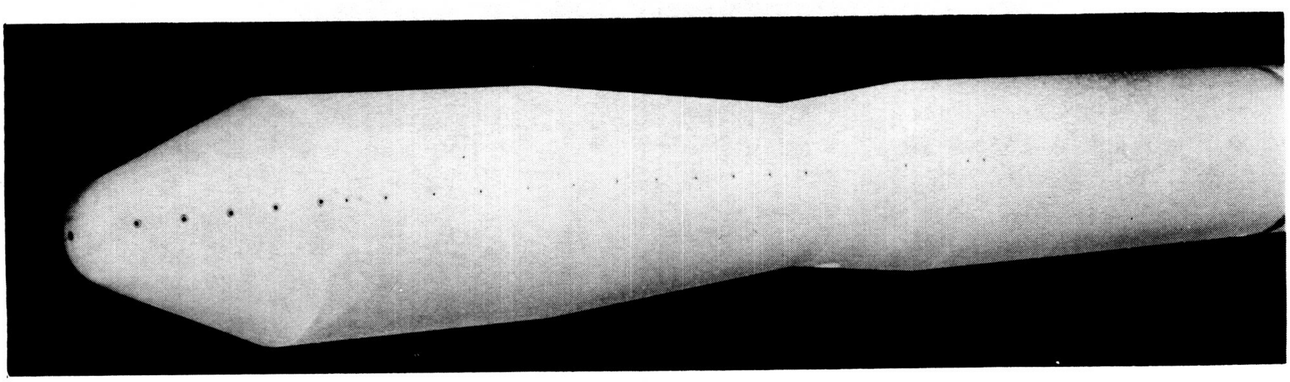

(c) Orifice installation. L-63-3830

Figure 2.- Model photographs.

with the single orifice row at roll angles ϕ of 0°, 22.5°, and 45° at equal positive and negative angles of attack. All tests were conducted through an angle-of-attack range from about -6° to 6° at Reynolds numbers per foot that varied from about 3.17×10^{6} at a Mach number of 0.60 to 4.22×10^{6} at a Mach number of 1.20. (See fig. 3.) The investigation was conducted with transition fixed at model station 2.89 inches by utilizing a transition strip that was 0.1 inch wide and was composed of No. 120 carborundum grains set in a plastic adhesive.

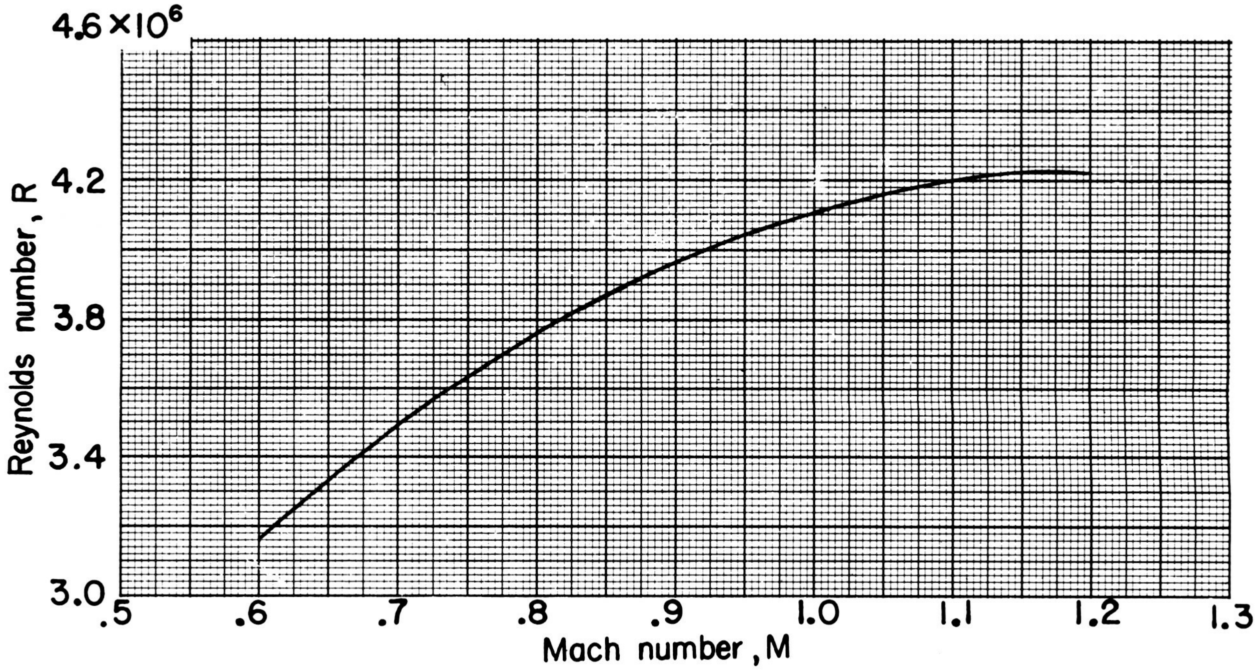

Figure 3.- Variation of average test Reynolds number per foot with Mach number.

Effects of subsonic boundary interference in the slotted test section are considered negligible, and no corrections for these effects have been applied. At supersonic speeds the data are generally affected by boundary-reflected disturbances, which occur at Mach numbers from slightly over 1.03 to those at which the disturbances are reflected downstream of the model base. For the force-test part of the present investigation, the model length and tunnel power restrictions precluded the attainment of a Mach number at which the model would be free from reflections. Therefore, no force-test results are presented for Mach numbers higher than 1.03. However, pressure-distribution results are presented for a Mach number of 1.20, since the reflections would occur well rearward on the model at this Mach number and would have no effect on the measured surface pressures.

Axial-force results have been adjusted to the condition of free-stream static pressure acting at the model base.

PRESENTATION OF RESULTS

A list of figures presenting results of this investigation is given below. In order to facilitate presentation of the data, staggered scales have been used in some of the figures, and care should be taken in selecting the proper zero axis for each curve. Center-of-pressure results are presented in terms of maximum body diameters forward of the model base.

DISCUSSION

Force and Moment Characteristics

Results of the force-test phase of the investigation are given in figures 4 to 7 and are summarized in figure 8. A comparison of the results presented in figure 8 with results given in reference 4 for the earlier Scout vehicle indicates that the effects of fin addition on the longitudinal characteristics are quantitatively similar for the two configurations, as would be expected.

Overall effects of the modification are illustrated in figure 9 by a comparison of the present results with those of reference 4 for the configuration having fins but no protuberances (configuration 215, ref. 4). The combined effects of the fourth-stage enlargement and the incidental changes mentioned previously are seen to result, generally, in a slight increase in the values of the normal-force-curve slope, a more noticeable increase in the values of the pitching-moment-curve slope, and a forward shift in the center-of-pressure location.

As would be expected, the greatest effects of the modification appear in the axial-force results (fig. 9(b)). Increases in the axial-force coefficients resulting from enlarging the upper section vary from about 15 percent at a Mach number of 0.60 to 42 percent at a Mach number of 1.03, the latter increase indicating the sizable increase in wave drag associated with the modified configuration. Little or no effects of the modification are apparent in the base axial-force characteristics.

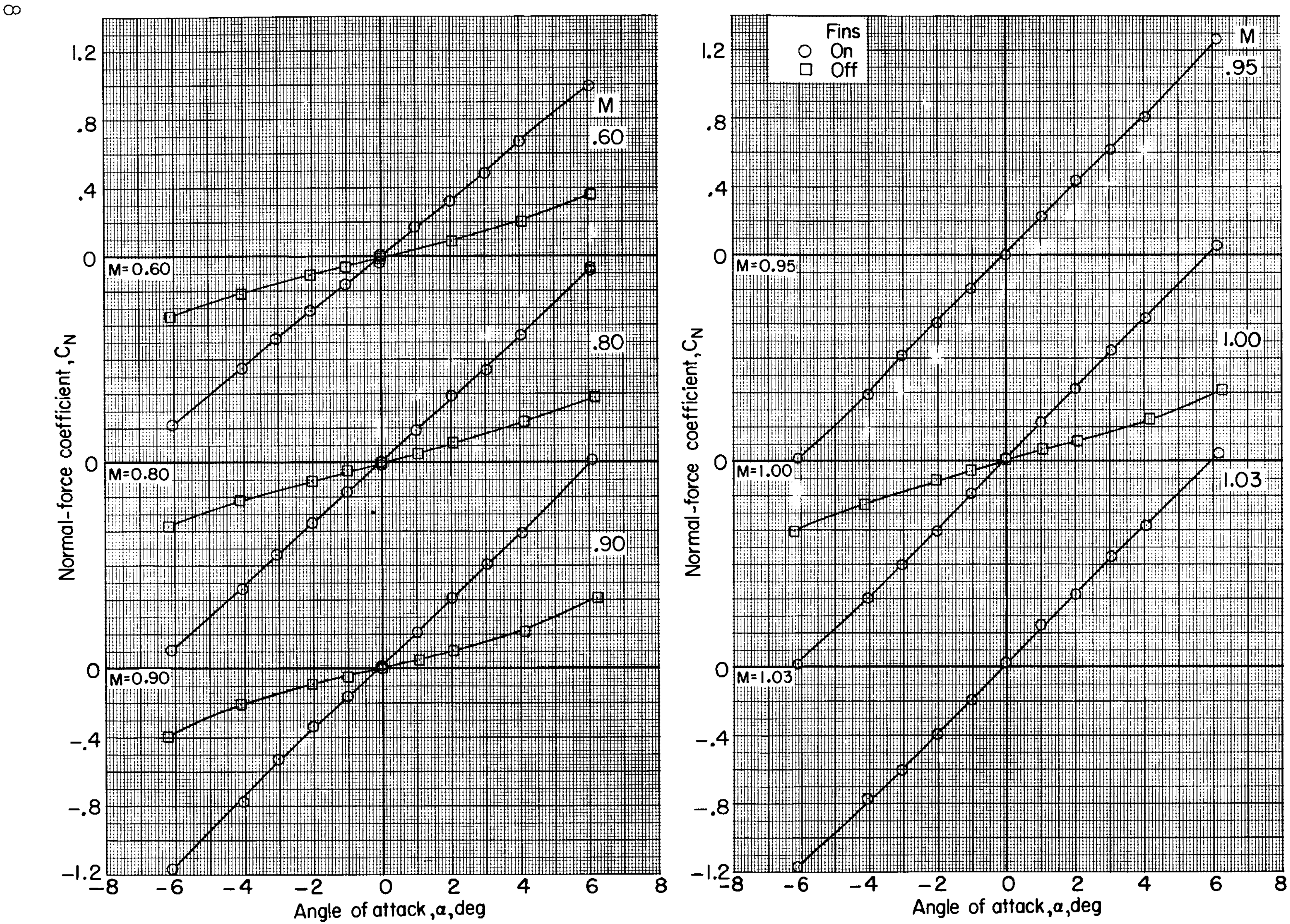

Figure 4.- Variation of normal-force coefficient with angle of attack.

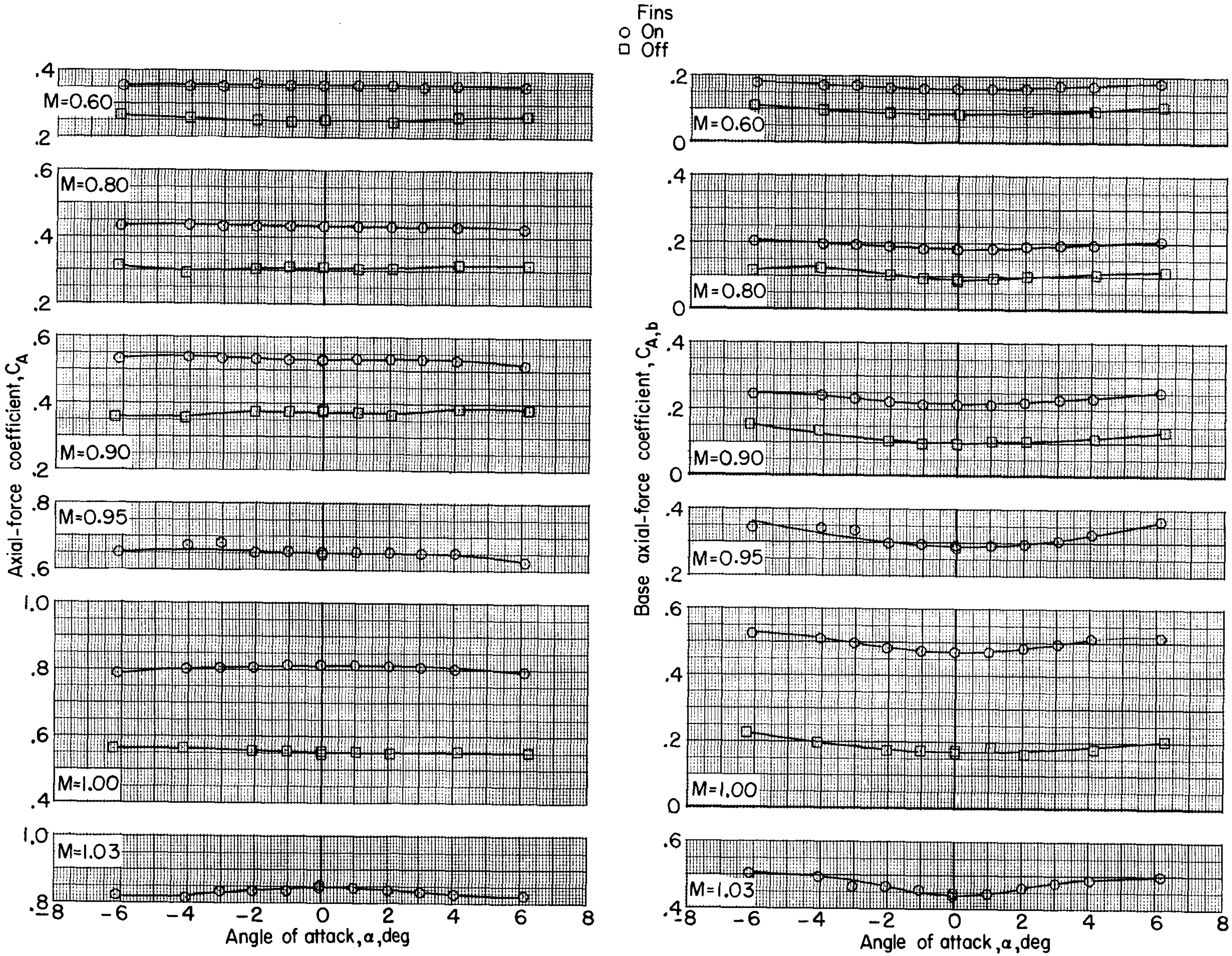

Figure 5.- Variation of axial-force coefficient with angle of attack.

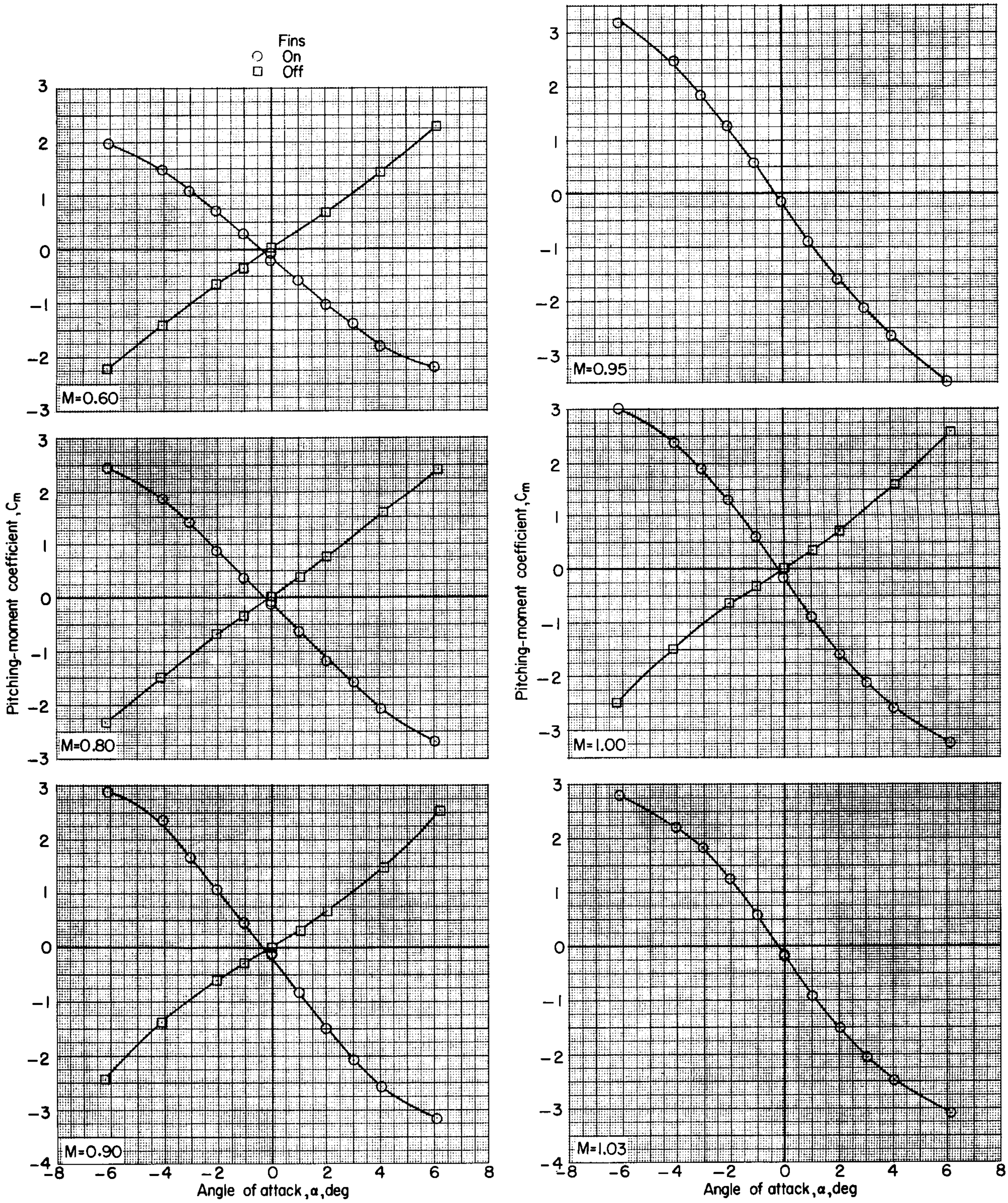

Figure 6.- Variation of pitching-moment coefficient with angle of attack.

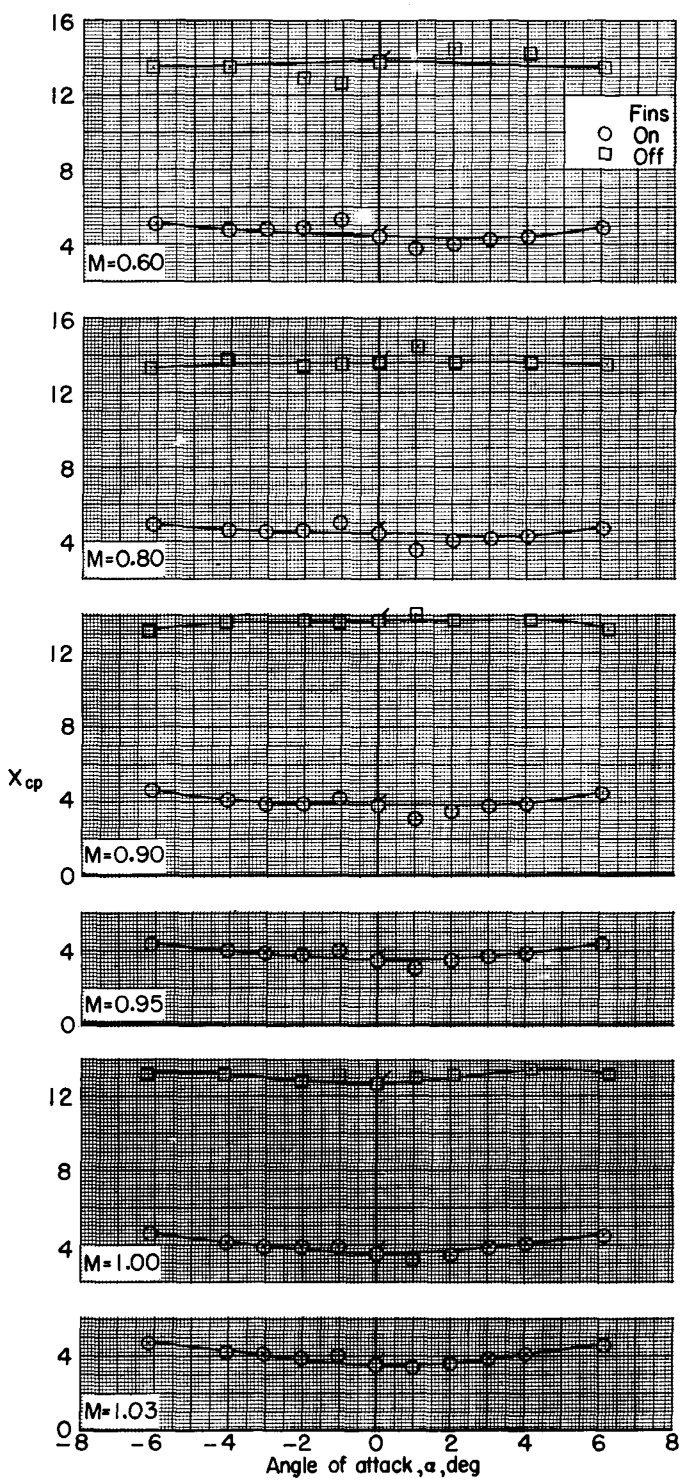

Figure 7.- Variation of center-of-pressure location with angle of attack. Flagged test points computed with C_{m_α} and C_{N_α} through zero angle of attack.

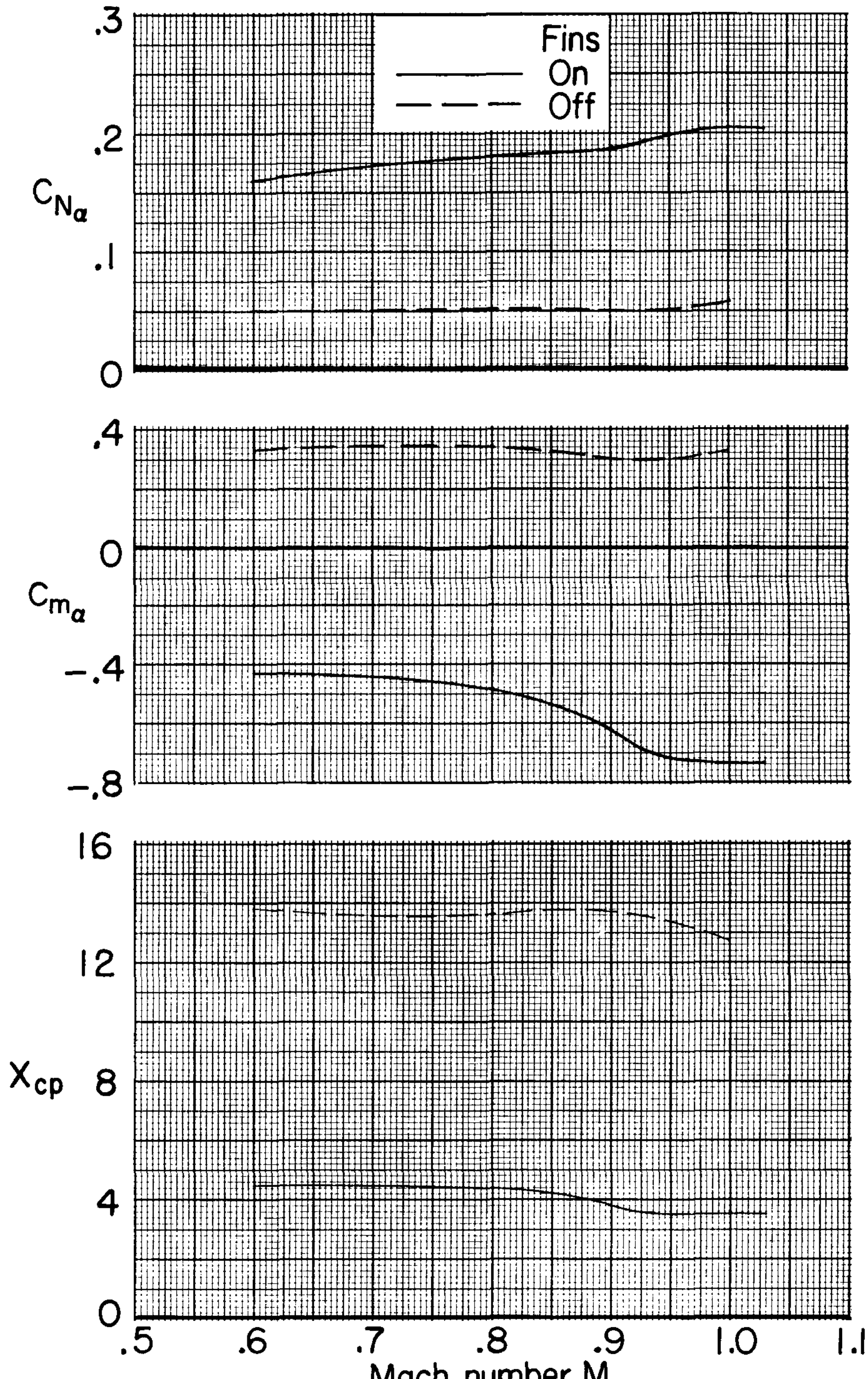

(a) C_{N_α}, C_{m_α}, and X_{cp} against Mach number.

Figure 8.- Summary of aerodynamic characteristics in pitch. $\alpha = 0^\circ$.

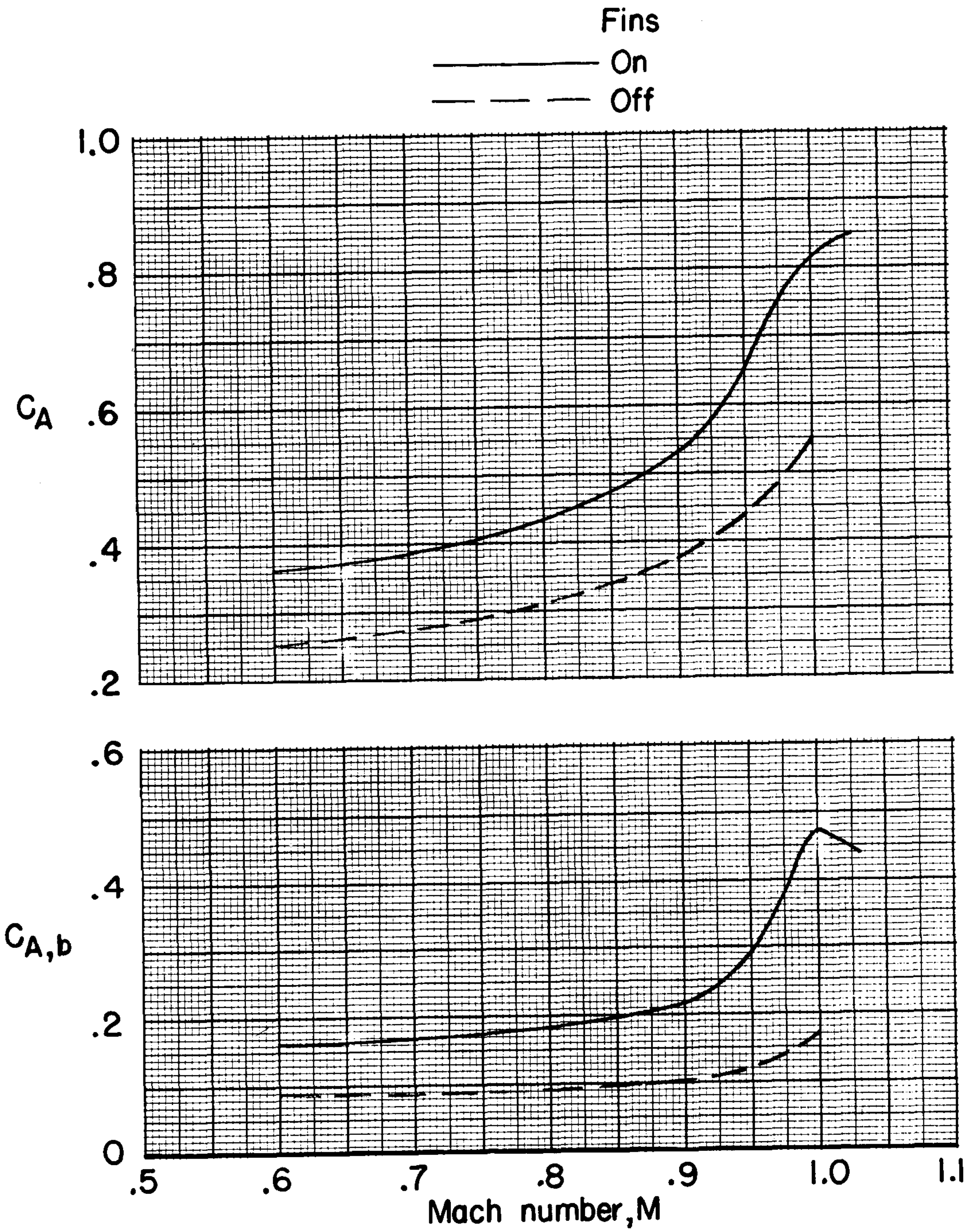

(b) C_A and $C_{A,b}$ against Mach number.

Figure 8.- Concluded.

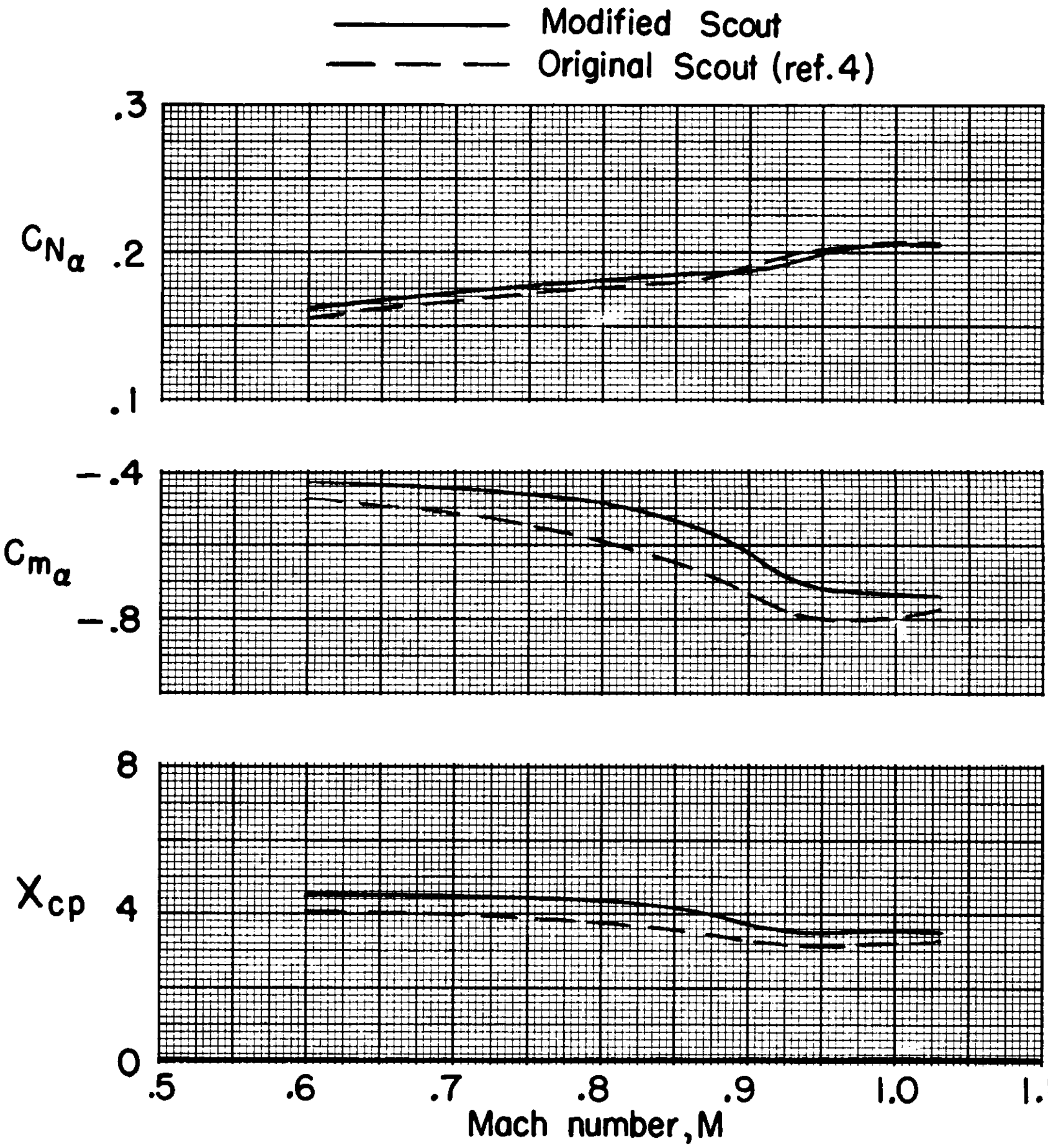

(a) C_{N_α}, C_{m_α}, and X_{cp} against Mach number.

Figure 9.- Comparison of modified and original Scout configurations. Fins on; protuberances off; $\alpha = 0^\circ$.

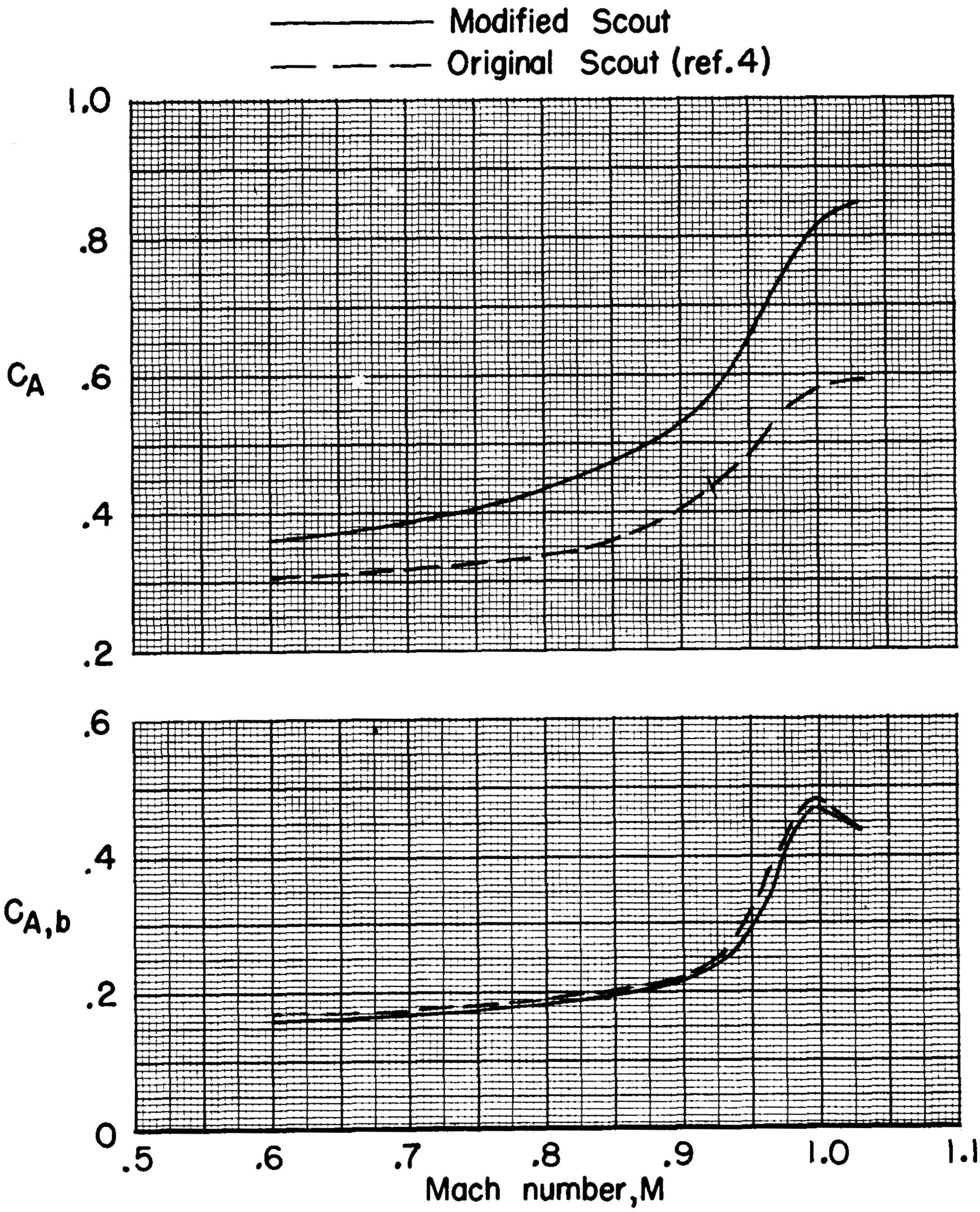

(b) C_A and $C_{A,b}$ against Mach number.

Figure 9.- Concluded.

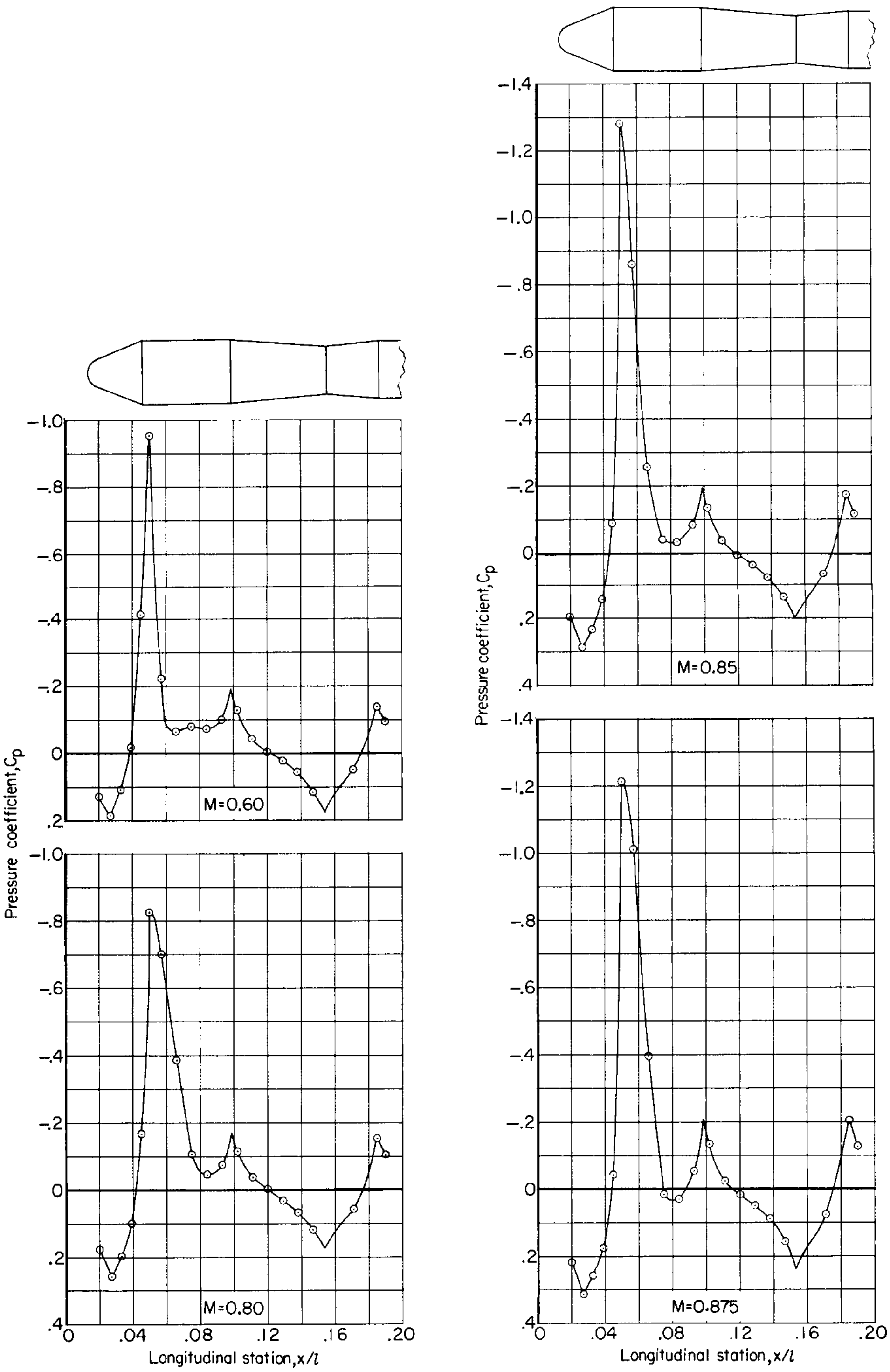

(a) M = 0.60 to 0.875.

Figure 10.- Surface pressure distributions for modified fourth stage at several Mach numbers. $\alpha = 0^{\circ}$; $\phi = 0^{\circ}$.

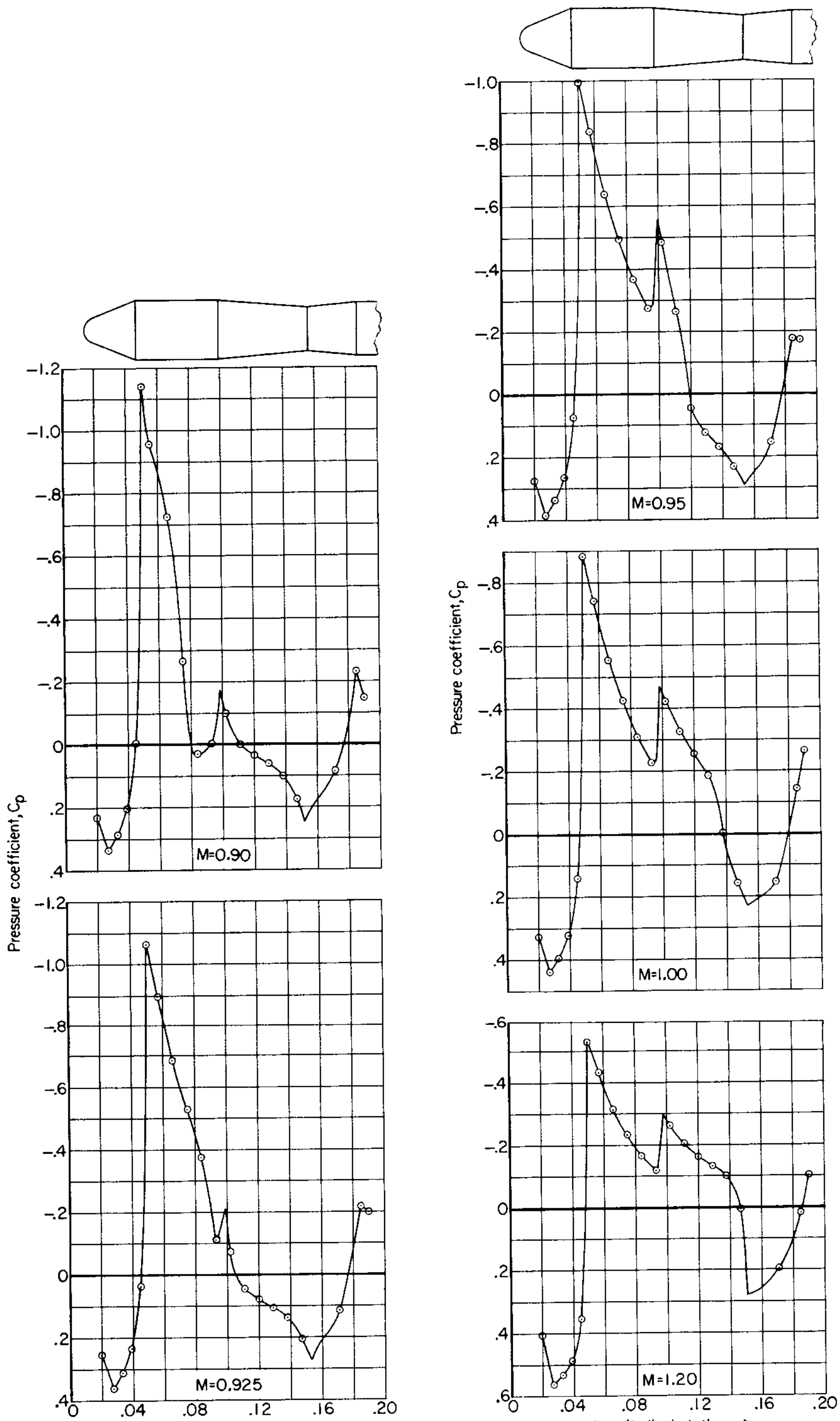

(b) M = 0.90 to 1.20.

Figure 10.- Concluded.

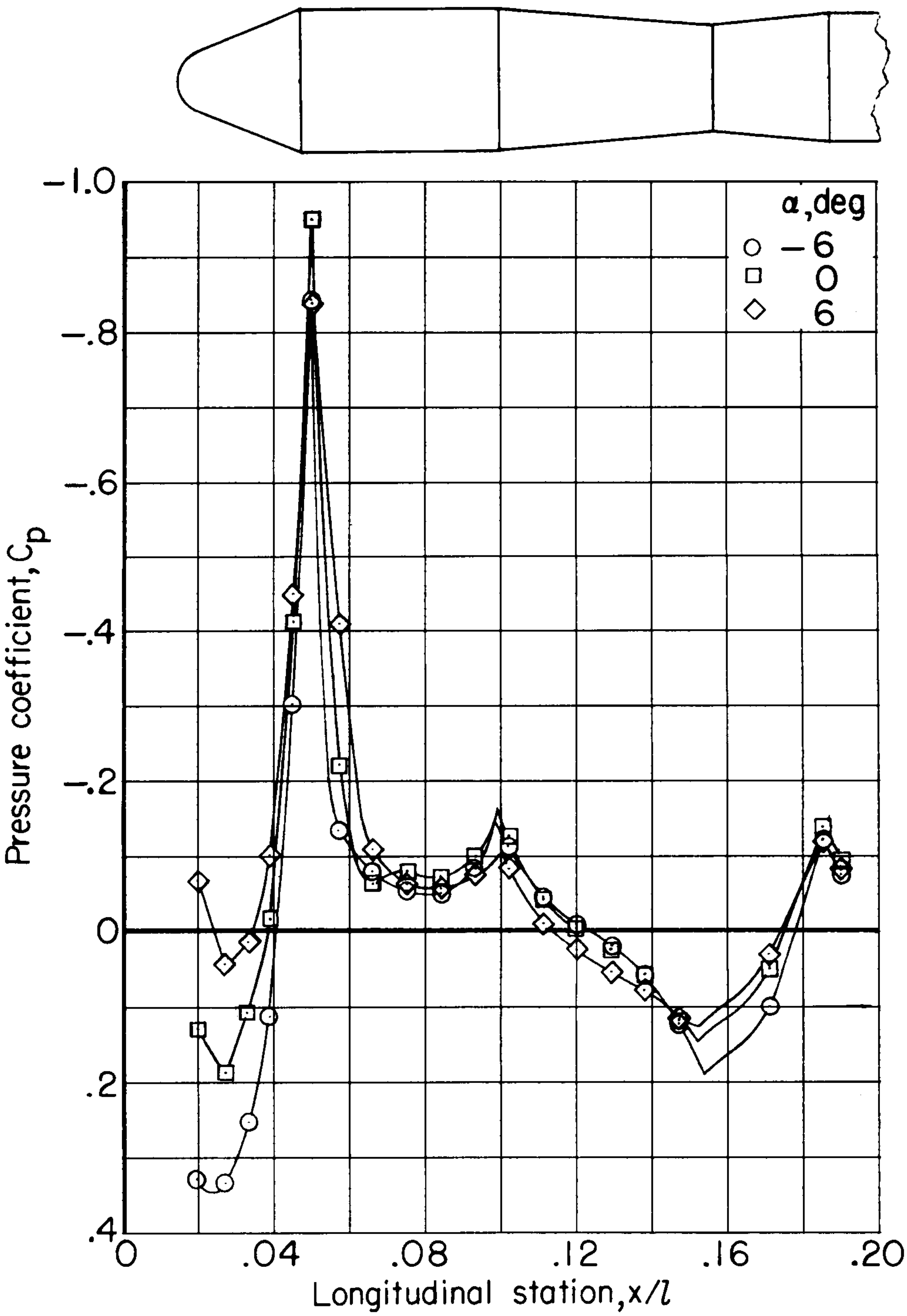

(a) M = 0.60.

Figure 11.- Effect of angle of attack on surface pressure distributions for modified fourth stage. $\phi = 0^{\circ}$.

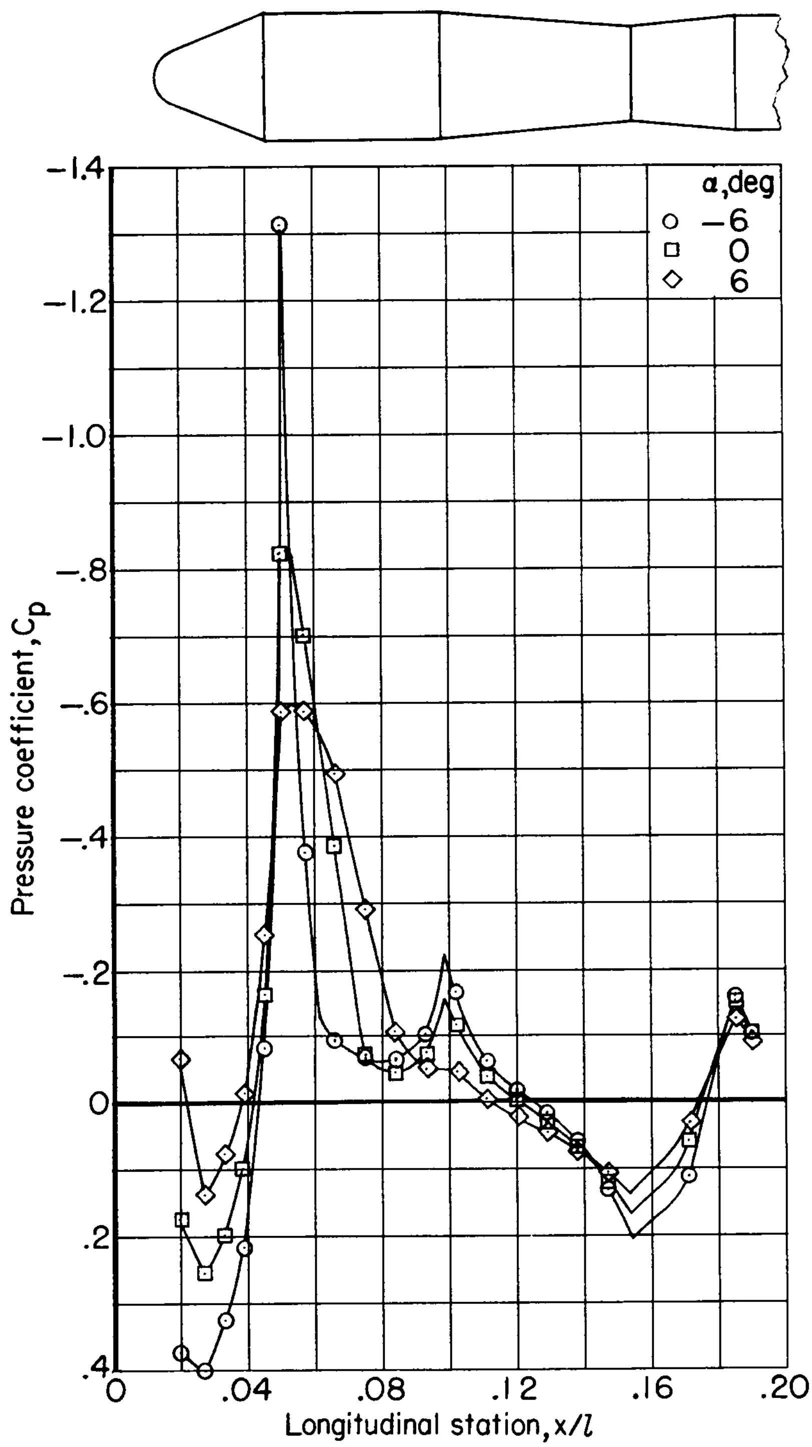

(b) M = 0.80.

Figure 11.- Continued.

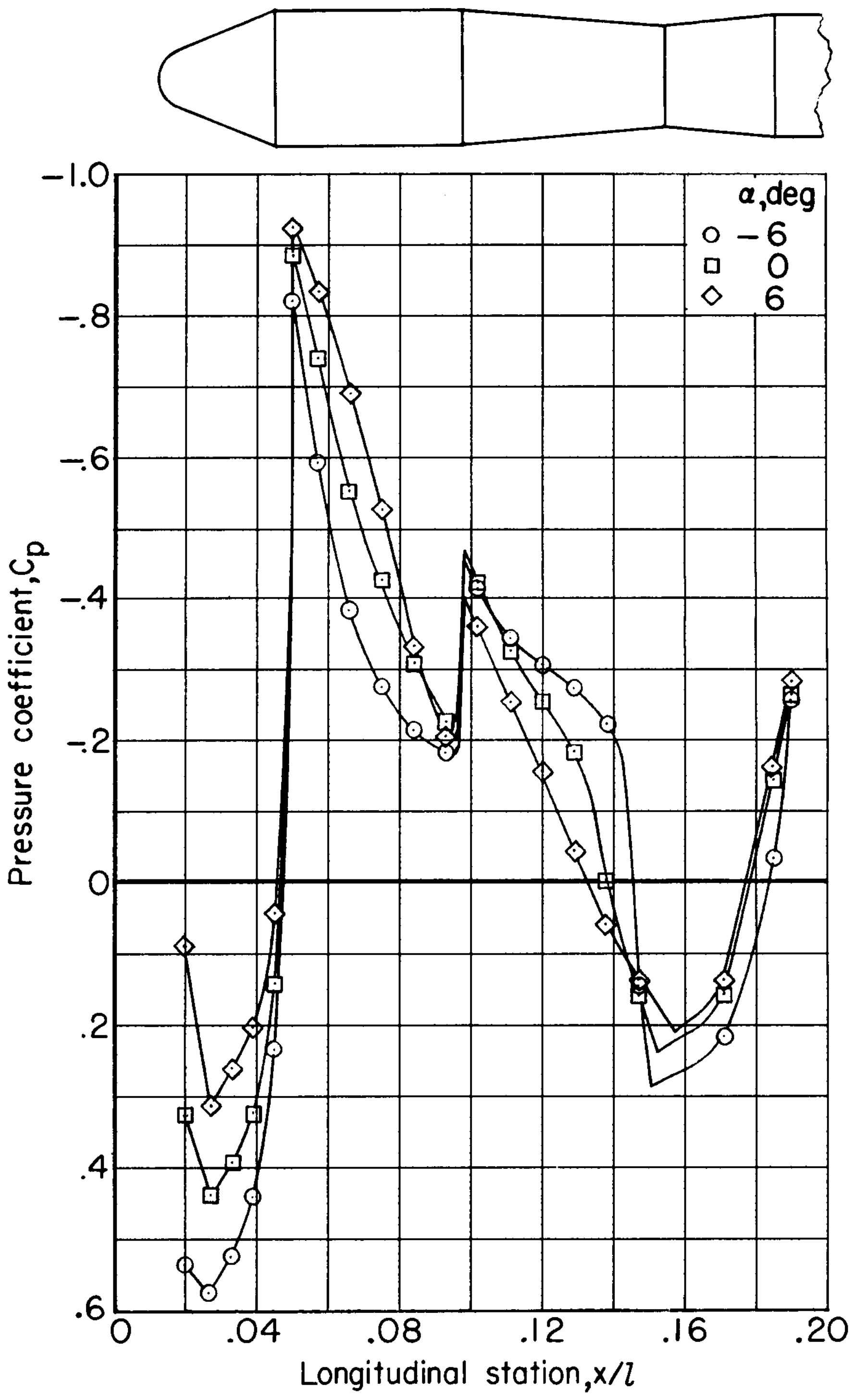

(c) M = 1.00.

Figure 11.- Continued.

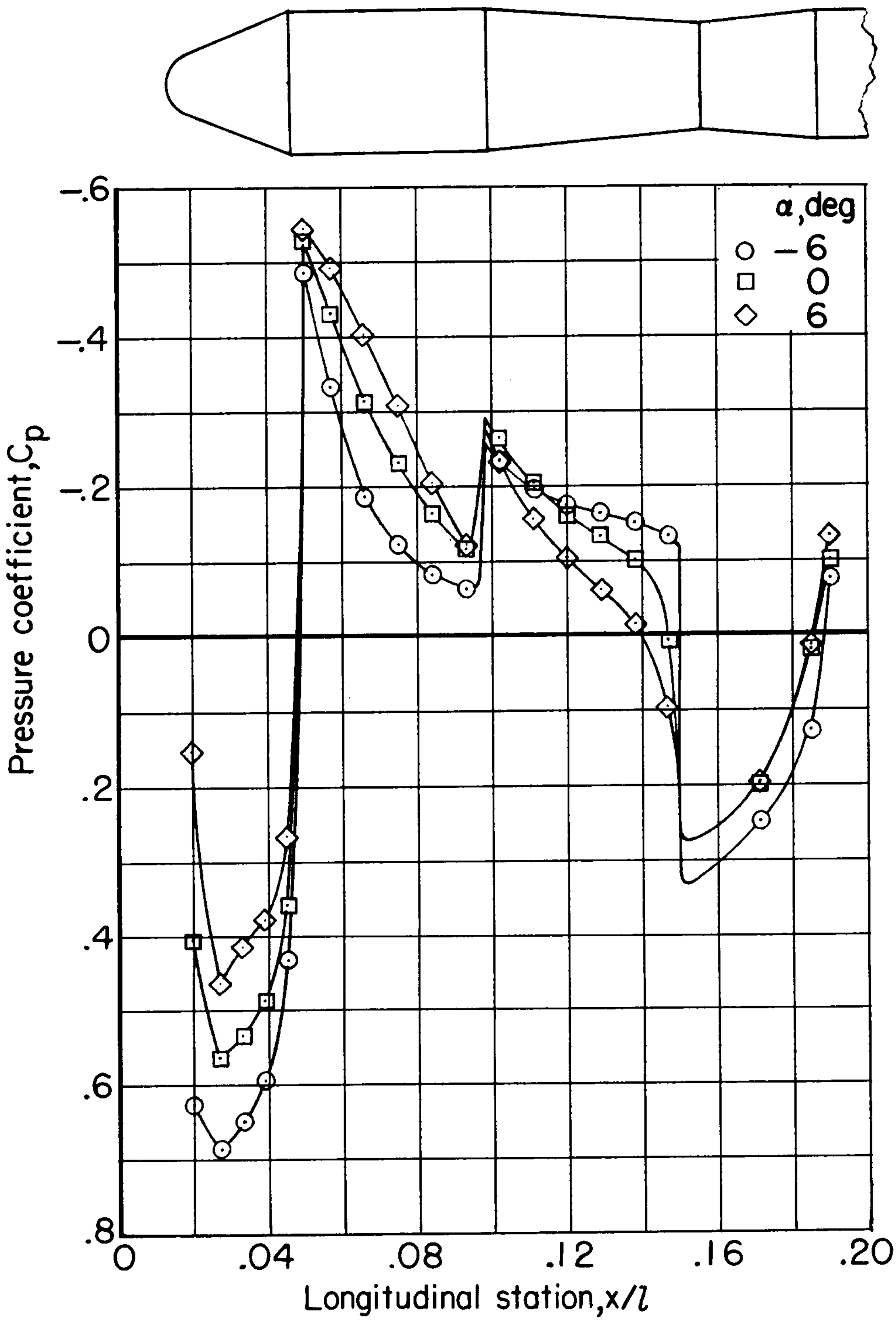

(d) M = 1.20.

Figure 11.- Concluded.

Surface Pressure Distributions

The effects of Mach number on the surface pressure distributions for the modified nose region are given in figure 10 for an angle of attack of 0°. It should be noted that the pressure coefficients obtained from the nose stagnation orifice ($x/l = 0.014$), although included in table I, are not presented on the pressure-distribution plots. The most noticeable effects of increasing Mach number appear as sizable variations in the negative pressure-coefficient peaks associated with the nose-cone—cylinder and cylinder—reverse-flare junctures. A fairly rapid broadening of these peaks is also apparent at the higher test Mach numbers. (For example, see results for $M = 0.875$ to $M = 0.95$.) As noted in references 6 and 8, such variations may impose local loads across the launch-vehicle outer structure (depending, of course, upon venting arrangements) that are significantly greater than those associated with the maximum dynamic-pressure condition in flight.

The effects of a variation in angle of attack from -6° to 6° are shown for several Mach numbers in figure 11. These results are for the condition for which the single orifice row extends along the model top surface ($\phi = 0^{\circ}$), and they indicate two points of interest. At a Mach number of 0.80 for the region just rearward of the nose-cone—cylinder juncture, evidences of increasing flow separation with increasing angle of attack are apparent in the lowering and broadening of the negative pressure-coefficient peaks. The second point of interest is associated with the region of the rear-facing transition flare, for which the results generally show that an increase in angle of attack is accompanied by an increase in surface pressures. Examination of the results presented in figure 11 and table I suggests that increases in angle of attack are accompanied by the presence of increasingly negative section normal-force coefficients over most of the length of the rear-facing transition flare.

SUMMARY OF RESULTS

An investigation at transonic Mach numbers of a 1/15-scale model of a modified four-stage Scout launch vehicle has indicated the following results:

1. A comparison of the present results with those presented in NASA Technical Note D-794 indicates that enlargement of the fourth stage causes a slight general increase in the values of the normal-force-curve slope, a more noticeable increase in the values of the pitching-moment-curve slope, and a slight forward shift in the center-of-pressure location.

2. Measurements of the surface-pressure distributions over the modified region indicate sizable variations of the negative pressure-coefficient peaks associated with the nose-cone—cylinder and cylinder—reverse-flare junctures with variations in Mach number or angle of attack.

3. Examination of the results suggests the presence of increasingly negative section normal-force coefficients over the region of the reverse flare with increases in angle of attack.

Langley Research Center,
National Aeronautics and Space Administration,
Langley Station, Hampton, Va., August 13, 1963.

REFERENCES

1. Jernell, Lloyd S., and Wong, Norman: Investigation of the Static Longitudinal Stability Characteristics of a 0.067-Scale Model of a Four-Stage Configuration of the Scout Research Vehicle at Mach Numbers of 2.29, 2.96, 3.96, and 4.65. NASA TN D-554, 1960.

2. Jernell, Lloyd S.: Investigation of the Static Longitudinal and Lateral Stability Characteristics of a 0.10-Scale Model of a Three-Stage Configuration of the Scout Research Vehicle at Mach Numbers of 2.29, 2.96, 3.96, and 4.65. NASA TN D-711, 1961.

3. Robinson, Ross B.: Aerodynamic Characteristics in Pitch and Sideslip of a 1/15-Scale Model of the Scout Vehicle at a Mach Number of 2.01. NASA TN D-793, 1961.

4. Kelly, Thomas C.: Transonic Wind-Tunnel Investigation of the Static Longitudinal Aerodynamic Characteristics of Several Configurations of the Scout Vehicle and of a Number of Related Models. NASA TN D-794, 1961.

5. Keynton, Robert J., and Fichter, Ann B.: Investigation of the Aerodynamic Characteristics of Two Preliminary Designs of Scout Research Vehicle at Mach Numbers From 1.77 to 4.65. NASA TN D-821, 1961.

6. Kelly, Thomas C.: Aerodynamic Loading Characteristics at Mach Numbers From 0.80 to 1.20 of a 1/10-Scale Three-Stage Scout Model. NASA TN D-945, 1961.

7. Jernell, Lloyd S.: Aerodynamic Loading Characteristics of a 1/10-Scale Model of the Three-Stage Scout Vehicle at Mach Numbers From 1.57 to 4.65. NASA TN D-1930, 1963.

8. Kelly, Thomas C.: Investigation at Transonic Mach Numbers of the Effects of Configuration Geometry on Surface Pressure Distributions for a Simulated Launch Vehicle. NASA TM X-845, 1963.

TABLE I.- PRESSURE COEFFICIENTS FOR MODIFIED SCOUT LAUNCH VEHICLE

(a) $\phi = 0^{\circ}$

$\alpha = -6^{\circ}$					
x/l	M = 0.60	M = 0.80	M = 0.90	M = 1.00	M = 1.20
0.014	1.074	1.157	1.204	1.258	1.389
.020	.328	.373	.430	.536	.625
.027	.332	.400	.466	.574	.684
.033	.251	.326	.403	.521	.649
.039	.111	.216	.312	.440	.593
.045	-.303	-.082	.076	.233	.433
.050	-.845	-1.313	-1.085	-.821	-.486
.057	-.137	-.378	-.807	-.594	-.333
.066	-.081	-.095	-.540	-.383	-.188
.075	-.055	-.067	-.273	-.276	-.123
.084	-.052	-.065	.007	-.215	-.082
.093	-.085	-.102	-.022	-.183	-.065
.102	-.133	-.169	-.219	-.414	-.235
.111	-.048	-.062	-.033	-.345	-.196
.120	-.011	-.017	.002	-.308	-.177
.129	.018	.015	.033	-.274	-.165
.138	.055	.057	.076	-.223	-.151
.147	.122	.132	.163	.144	-.133
.171	.100	.112	.139	.215	.247
.185	-.125	-.162	-.171	-.034	.125
.190	-.077	-.104	-.143	-.258	-.077

$\alpha = -3^{\circ}$					
x/l	M = 0.60	M = 0.80	M = 0.90	M = 1.00	M = 1.20
0.014	1.089	1.169	1.219	1.272	1.402
.020	.218	.276	.330	.418	.516
.027	.247	.326	.397	.493	.621
.033	.170	.259	.341	.440	.591
.039	.037	.152	.254	.367	.540
.045	-.362	-.127	.030	.174	.395
.050	-.963	-.993	-1.119	-.866	-.509
.057	-.170	-.672	-.892	-.684	-.386
.066	-.103	-.192	-.642	-.487	-.253
.075	-.077	-.050	-.271	-.369	-.179
.084	-.074	-.052	.028	-.284	-.128
.093	-.103	-.095	-.015	-.225	-.098
.102	-.140	-.149	-.134	-.436	-.254
.111	-.055	-.050	-.022	-.357	-.209
.120	-.018	-.012	.013	-.302	-.181
.129	.011	.020	.043	-.252	-.158
.138	.048	.062	.085	-.118	-.135
.147	.107	.129	.165	.146	-.096
.171	.063	.082	.108	.172	.223
.185	-.148	-.169	-.213	-.099	.077
.190	-.100	-.114	-.145	-.288	-.096

$\alpha = 0^{\circ}$									
x/l	M = 0.60	M = 0.80	M = 0.85	M = 0.875	M = 0.90	M = 0.925	M = 0.95	M = 1.00	M = 1.20
0.014	1.092	1.172	1.198	1.207	1.221	1.236	1.251	1.276	1.404
.020	.129	.174	.195	.214	.230	.253	.275	.327	.404
.027	.185	.256	.285	.312	.334	.361	.386	.438	.563
.033	.107	.197	.232	.258	.282	.310	.335	.391	.532
.039	-.018	.100	.143	.174	.204	.232	.263	.321	.486
.045	-.413	-.169	-.090	-.045	-.007	.034	.072	.140	.354
.050	-.952	-.826	-1.280	-1.212	-1.141	-1.068	-.996	-.886	-.530
.057	-.221	-.701	-.860	-1.011	-.959	-.899	-.838	-.742	-.432
.066	-.066	-.388	-.257	-.399	-.725	-.684	-.639	-.556	-.314
.075	-.081	-.107	-.041	.013	-.269	-.530	-.497	-.426	-.232
.084	-.074	-.045	.034	.029	.030	-.376	-.368	-.310	-.165
.093	-.100	-.077	-.083	-.053	-.002	-.112	-.275	-.227	-.119
.102	-.129	-.117	-.136	-.136	-.100	-.072	-.485	-.422	-.263
.111	-.044	-.040	-.037	-.024	.000	.046	-.263	-.327	-.204
.120	-.007	-.002	.002	.016	.033	.078	.047	-.256	-.163
.129	.022	.030	.034	.049	.061	.103	.123	-.185	-.133
.138	.055	.065	.074	.089	.100	.137	.170	-.002	-.100
.147	.114	.119	.136	.156	.174	.205	.232	.158	.005
.171	.048	.057	.064	.073	.085	.114	.154	.154	.198
.185	-.140	-.154	-.175	-.203	-.232	-.219	-.179	-.146	.018
.190	-.096	-.107	-.117	-.129	-.148	-.200	-.174	-.264	-.100

$\alpha = 3^{\circ}$					
x/l	M = 0.60	M = 0.80	M = 0.90	M = 1.00	M = 1.20
0.014	1.085	1.164	1.217	1.266	1.396
.020	.033	.060	.111	.209	.279
.027	.129	.201	.273	.377	.509
.033	.066	.137	.219	.331	.474
.039	-.055	.042	.143	.264	.432
.045	-.435	-.211	-.052	.097	.311
.050	-.875	-.644	-1.165	-.903	-.542
.057	-.295	-.622	-1.015	-.789	-.467
.066	-.103	-.493	-.805	-.623	-.361
.075	-.077	-.249	-.191	-.475	-.275
.084	-.070	-.080	-.007	-.327	-.193
.093	-.092	-.052	.013	-.217	-.128
.102	-.107	-.072	-.061	-.391	-.256
.111	-.026	-.020	.017	-.284	-.188
.120	.011	.012	.052	-.199	-.135
.129	.041	.040	.080	-.081	-.096
.138	.070	.070	.117	.065	-.054
.147	.114	.109	.176	.162	.082
.171	.037	.042	.069	.142	.186
.185	-.125	-.132	-.206	-.166	-.014
.190	-.089	-.095	-.139	-.229	-.093

$\alpha = 6^{\circ}$					
x/l	M = 0.60	M = 0.80	M = 0.90	M = 1.00	M = 1.20
0.014	1.055	1.139	1.195	1.249	1.379
.020	-.070	-.067	-.013	.087	.151
.027	.041	.137	.215	.310	.461
.033	.011	.077	.158	.260	.414
.039	-.103	-.015	.087	.201	.375
.045	-.450	-.254	-.098	.041	.263
.050	-.804	-.587	-1.180	-.925	-.544
.057	-.410	-.587	-1.063	-.836	-.491
.066	-.111	-.495	-.443	-.690	-.402
.075	-.066	-.291	-.286	-.529	-.309
.084	-.059	-.109	-.102	-.331	-.205
.093	-.074	-.050	.017	-.207	-.121
.102	-.085	-.047	-.002	-.361	-.233
.111	-.011	-.005	.041	-.252	-.158
.120	.022	.022	.069	-.158	-.105
.129	.052	.047	.095	-.045	-.061
.138	.077	.072	.124	.059	-.018
.147	.114	.102	.169	.132	.095
.171	.030	.032	.056	.134	.195
.185	-.122	-.127	-.191	-.164	.014
.190	-.085	-.092	-.128	-.282	-.132

TABLE I.- PRESSURE COEFFICIENTS FOR MODIFIED SCOUT LAUNCH VEHICLE - Continued

(b) $\phi = 22.5^{\circ}$

$\alpha = -6^{\circ}$			
x/l	M = 0.60	M = 0.90	M = 1.20
0.014	1.074	1.204	1.386
.020	.305	.423	.607
.027	.309	.460	.670
.033	.232	.397	.631
.039	.092	.304	.573
.045	-.324	.074	.420
.050	-.875	-1.089	-.497
.057	-.151	-.824	-.344
.066	-.096	-.555	-.201
.075	-.074	-.382	-.131
.084	-.070	-.015	-.094
.093	-.099	-.022	-.077
.102	-.147	-.217	-.245
.111	-.062	-.026	-.206
.120	-.026	.007	-.189
.129	.004	.037	-.171
.138	.040	.078	-.140
.147	.107	.165	-.142
.171	.081	.137	.236
.185	-.143	-.174	.117
.190	-.081	-.171	-.080

$\alpha = -3^{\circ}$			
x/l	M = 0.60	M = 0.90	M = 1.20
0.014	1.088	1.221	1.397
.020	.213	.321	.510
.027	.246	.388	.617
.033	.165	.332	.587
.039	.037	.245	.535
.045	-.368	.024	.392
.050	-.974	-1.130	-.510
.057	-.169	-.900	-.388
.066	-.103	-.657	-.255
.075	-.081	-.243	-.182
.084	-.077	.033	-.129
.093	-.103	-.015	-.100
.102	-.143	-.137	-.259
.111	-.055	-.020	-.212
.120	-.018	.013	-.182
.129	.011	.043	-.161
.138	.044	.085	-.129
.147	.110	.165	-.101
.171	.062	.104	.220
.185	-.147	-.219	.075
.190	-.088	-.137	-.091

$\alpha = 0^{\circ}$			
x/l	M = 0.60	M = 0.90	M = 1.20
0.014	1.092	1.223	1.400
.020	.129	.228	.407
.027	.184	.332	.565
.033	.114	.273	.531
.039	-.015	.200	.484
.045	-.393	-.009	.351
.050	-.949	-1.148	-.530
.057	-.250	-.967	-.432
.066	-.099	-.744	-.312
.075	-.081	-.262	-.229
.084	-.077	.041	-.164
.093	-.099	.002	-.119
.102	-.129	-.100	-.264
.111	-.044	.004	-.206
.120	-.007	.035	-.166
.129	.026	.065	-.136
.138	.059	.104	-.100
.147	.114	.176	-.002
.171	.048	.085	.198
.185	-.140	-.234	.017
.190	-.088	-.137	-.093

$\alpha = 3^{\circ}$			
x/l	M = 0.60	M = 0.90	M = 1.20
0.014	1.085	1.213	1.395
.020	.040	.126	.287
.027	.125	.278	.510
.033	.066	.219	.474
.039	-.055	.141	.432
.045	-.426	-.059	.309
.050	-.923	-1.176	-.545
.057	-.312	-1.026	-.467
.066	-.103	-.792	-.362
.075	-.077	-.163	-.274
.084	-.074	.015	-.196
.093	-.096	.011	-.133
.102	-.110	-.069	-.264
.111	-.033	.017	-.196
.120	.004	.050	-.143
.129	.033	.078	-.100
.138	.066	.115	-.061
.147	.110	.176	.079
.171	.037	.067	.184
.185	-.250	-.206	-.019
.190	-.085	-.126	-.089

$\alpha = 6^{\circ}$			
x/l	M = 0.60	M = 0.90	M = 1.20
0.014	1.059	1.191	1.376
.020	-.062	-.011	.145
.027	.077	.204	.458
.033	.011	.150	.416
.039	-.103	.076	.379
.045	-.460	-.106	.271
.050	-.846	-1.206	-.559
.057	-.375	-1.080	-.495
.066	-.107	-.573	-.397
.075	-.077	-.278	-.306
.084	-.070	-.067	-.213
.093	-.088	.013	-.135
.102	-.096	-.037	-.253
.111	-.022	.026	-.175
.120	.015	.052	-.119
.129	.040	.078	-.077
.138	.070	.108	-.031
.147	.107	.158	.087
.171	.022	.037	.166
.185	-.250	-.219	-.023
.190	-.085	-.141	-.098

TABLE I.- PRESSURE COEFFICIENTS FOR MODIFIED SCOUT LAUNCH VEHICLE - Concluded

(c) $\phi = 45^\circ$

$\alpha = -6^\circ$			
x/l	M = 0.60	M = 0.90	M = 1.20
0.014	1.077	1.205	1.389
.020	.250	.361	.552
.027	.265	.400	.622
.033	.184	.341	.592
.039	.051	.253	.539
.045	-.363	.106	.392
.050	-.834	-1.117	-.511
.057	-.180	-.870	-.371
.066	-.118	-.596	-.238
.075	-.096	-.225	-.159
.084	-.088	.002	-.119
.093	-.118	-.043	-.098
.102	-.132	-.188	-.233
.111	-.074	-.041	-.228
.120	-.037	-.006	-.207
.129	-.007	.022	-.186
.138	.029	.065	-.166
.147	.092	.147	-.145
.171	.055	.104	.212
.185	-.165	-.205	.091
.190	-.103	-.145	-.100

$\alpha = -3^\circ$			
x/l	M = 0.60	M = 0.90	M = 1.20
0.014	1.092	1.220	1.399
.020	.187	.296	.482
.027	.224	.369	.601
.033	.151	.311	.571
.039	.018	.227	.522
.045	-.390	.013	.380
.050	-.904	-1.132	-.518
.057	-.187	-.916	-.401
.066	-.114	-.670	-.270
.075	-.085	-.263	-.193
.084	-.081	.028	-.140
.093	-.107	-.017	-.109
.102	-.118	-.104	-.235
.111	-.005	-.017	-.217
.120	-.022	.015	-.187
.129	.011	.043	-.158
.138	.044	.086	-.124
.147	.107	.164	-.091
.171	.051	.095	.210
.185	-.151	-.229	.063
.190	-.096	-.138	-.096

$\alpha = 0^\circ$			
x/l	M = 0.60	M = 0.90	M = 1.20
0.014	1.096	1.222	1.403
.020	.121	.218	.394
.027	.184	.328	.560
.033	.110	.274	.531
.039	-.015	.192	.485
.045	-.404	-.015	.352
.050	-.956	-1.149	-.529
.057	-.235	-.965	-.433
.066	-.103	-.730	-.313
.075	-.081	-.192	-.231
.084	-.074	.032	-.165
.093	-.099	-.004	-.117
.102	-.103	-.084	-.233
.111	-.040	.002	-.203
.120	-.004	.030	-.163
.129	.026	.060	-.131
.138	.059	.099	-.096
.147	.114	.171	.004
.171	.048	.080	.200
.185	-.134	-.229	.016
.190	-.088	-.136	-.091

$\alpha = 3^\circ$			
x/l	M = 0.60	M = 0.90	M = 1.20
0.014	1.085	1.218	1.403
.020	.051	.147	.394
.027	.132	.289	.560
.033	.062	.238	.531
.039	-.059	.160	.485
.045	-.426	-.037	.352
.050	-.937	-1.151	-.529
.057	-.290	-.998	-.433
.066	-.107	-.775	-.313
.075	-.085	-.192	-.231
.084	-.077	.019	-.165
.093	-.099	.013	-.117
.102	-.099	-.052	-.233
.111	-.037	.019	-.203
.120	.000	.052	-.163
.129	.029	.082	-.131
.138	.059	.119	-.096
.147	.107	.181	.004
.171	.033	.073	.200
.185	-.136	-.220	.016
.190	-.088	-.130	-.091

$\alpha = 6^\circ$			
x/l	M = 0.60	M = 0.90	M = 1.20
0.014	1.063	1.194	1.380
.020	-.026	.041	.152
.027	.081	.229	.455
.033	.015	.179	.429
.039	-.103	.106	.392
.045	-.441	-.076	.284
.050	-.879	-1.173	-.553
.057	-.368	-1.039	-.485
.066	-.114	-.829	-.382
.075	-.088	-.242	-.292
.084	-.081	-.032	-.214
.093	-.099	-.015	-.156
.102	-.092	-.045	-.254
.111	-.033	.024	-.203
.120	.004	.054	-.144
.129	.033	.080	-.100
.138	.062	.114	-.051
.147	.107	.171	.086
.171	.018	.043	.156
.185	-.140	-.229	-.032
.190	-.096	-.140	-.077

NASA-Langley, 1963 L-3549